Analytical and Bioanalytical Chemistry (2024) 416:1667–1677
https://doi.org/10.1007/s00216-024-05172-5

RESEARCH PAPER

DNA aptamer-linked sandwich structure enhanced SPRi sensor for rapid, sensitive, and quantitative detection of SARS-CoV-2 spike protein

Rengang Sun[1] · Yadong Zhou[1] · Yunzhu Fang[1] · Yirui Qin[1] · Yekai Zheng[1] · Li Jiang[1]

Received: 22 November 2023 / Revised: 23 January 2024 / Accepted: 24 January 2024 / Published online: 12 February 2024
© The Author(s), under exclusive licence to Springer-Verlag GmbH, DE part of Springer Nature 2024

Abstract

The harm and impact of the COVID-19 pandemic have highlighted the importance of fast, sensitive, and cost-effective virus detection methods. In this study, we developed a DNA aptamer sensor using nanoparticle-enhanced surface plasmon resonance imaging (SPRi) technology to achieve efficient labeling-free detection of SARS-CoV-2 S protein. We used the same DNA aptamer to modify the surface of the SPRi sensor chip and gold nanoparticles (AuNPs), respectively, for capturing target analytes and amplifying signals, achieving ideal results while greatly reducing costs and simplifying the preparation process. The SPRi sensing method exhibits a good linear relationship ($R^2 = 0.9926$) in the concentration range of 1–20 nM before adding AuNPs to amplify the signal, with a limit of detection (LOD) of 0.32 nM. After amplifying the signal, there is a good linear relationship ($R^2 = 0.9829$) between the concentration range of 25–1000 pM, with a LOD of 5.99 pM. The simulation results also verified the effectiveness of AuNPs in improving SPRi signal response. The SPRi sensor has the advantage of short detection time and can complete the detection within 10 min. In addition, the specificity and repeatability of this method can achieve excellent results. This is the first study to simultaneously capture a viral marker protein and amplify the signal using polyadenylic acid (polyA)–modified DNA aptamers on the SPR platform. This scheme can be used as a fast and inexpensive detection method for diagnosis at the point of care (POC) to combat current and future epidemics caused by the virus.

Keywords Surface plasmon resonance imaging (SPRi) · Sensor · SARS-CoV-2 S protein · PolyA-modified DNA aptamer · Gold nanoparticles (AuNPs)

Introduction

The coronavirus disease 2019 (COVID-19) poses a serious threat to global human health and seriously affects economic and social development [1]. Humanity has made some progress in the fight against the epidemic. The World Health Organization recently announced that the COVID-19 pandemic no longer constitutes a "public health emergency of international concern" and lifted the highest-level alert. However, the Director General of the World Health Organization Tedros Adhanom Ghebreyesus also said that this does not mean that the COVID-19 epidemic as a global health threat has ended. Undoubtedly, people still need to continue to fight against severe acute respiratory syndrome coronavirus 2 (SARS-CoV-2) and potential new viruses.

SARS-CoV-2 belongs to the β coronavirus genus and has a sense single-stranded RNA (+ssRNA) as genetic material. The RNA can encode 27 proteins and four structural proteins with specific functions: nucleocapsid protein (N), membrane protein (M), envelope protein (E), and spike protein (S) [2]. Among them, the S protein binds to the host cell receptor angiotensin-converting enzyme 2 (ACE2) through its receptor-binding domain (RBD), promoting the entry of the virus into the host cell [3, 4]. Compared to other β coronavirus genuses, SARS-CoV-2 has lower N protein expression and higher S protein expression, and SARS-CoV-2 S protein has a higher affinity for ACE2 [5]. It may lead to SARS-CoV-2 being more infectious than previous viruses. Therefore, the S

✉ Yadong Zhou
zyadong2013@cjlu.edu.cn

✉ Li Jiang
lijiang@cjlu.edu.cn

[1] College of Optical and Electronic Technology, China Jiliang University, Hangzhou 310018, China

protein and its RBD region are key targets for SARS-CoV-2 therapy, vaccines, and testing [6].

At present, commonly used methods to detect SARS-CoV-2 include real-time reverse transcription polymerase chain reaction (RT-PCR), enzyme-linked immunosorbent assay (ELISA), and lateral flow immunoassay (LFA) [7, 8]. RT-PCR is the gold standard for SARS-CoV-2 detection, with high sensitivity and specificity. However, this method is costly and time-consuming (at least 3 h) and requires operators to have a lot of technical skill, and there is a risk of contamination during the operation, making it difficult to apply at POC [8]. Similarly, ELISA also has the disadvantages of long time and high cost, while LFA has lower sensitivity and cannot detect early viruses [9, 10]. Therefore, it is necessary to develop new strategies to develop simple, fast, accurate, efficient, and affordable detection systems.

In this situation, biosensors are the ideal choice to provide alternative and reliable solutions for clinical diagnosis, real-time detection, and continuous monitoring. In the field of detecting viral markers, common biosensors include electrochemical, surface-enhanced Raman scattering (SERS), and surface plasmon resonance imaging (SPRi) sensors [11]. For example, Seo et al. [12] used anti-S protein antibodies that can bind SARS-CoV-2 virus particles to produce graphene-based field effect transistor (FET) electrochemical biosensors. These FET biosensors can respond to 16 pfu/mL of virus particles in PBS within 10 min. Yang et al. [13] developed a SERS sensor with a "virus trap" that utilizes ACE2's high affinity for SARS-CoV-2 S protein, which can detect SARS-CoV-2 pseudoviruses with a minimum concentration of 80 copies/mL in complex environments. However, these devices still have certain limitations, such as complex production processes and long detection times.

In recent years, SPRi biosensors have shown high sensitivity and fast and reliable diagnostic capabilities, which can be used to detect various pathogenic microorganisms, including coronavirus [11, 14–16]. Due to the high sensitivity of surface plasmon resonance (SPR) to the refractive index of metal surface dielectrics, significant changes in resonance parameters (such as phase, angle, reflected light intensity) occur when the refractive index of the material above the surface changes. At this point, through pixel-by-pixel monitoring using a CCD camera, the interaction between biomolecules on the metal surface can be analyzed, which is known as SPRi [17]. In addition, the application of new nanomaterials, such as AuNPs, magnetic nanoparticles, and quantum dots, can enhance the performance of SPRi sensors. For example, Qu et al. [18] developed a sensor based on fiber optic surface plasmon resonance (FO-SPR), which immobilizes labeled antigen onto the FO probe and amplifies the SPR signal using antibody-modified AuNPs. Huang et al. [19] prepared a nano SPR sensor; because of its periodic nanostructure design, it can easily observe changes in SPR wavelength and intensity through transmission spectroscopy or imaging.

Aptamer is a synthetic single-stranded DNA or RNA oligonucleotide with biorecognition properties, similar to antibodies. Due to electrostatic interactions and complementary conformations, it recognizes and binds to specific target molecules [20]. Compared with antibodies, aptamers have unique advantages such as low cost, no batch differences, strong stability, and high specificity [21]. In addition, aptamers can be easily chemically modified, making them easy to embed into various sensor materials or devices, capturing target molecules with high specificity and affinity [22]. For single-stranded nucleotides, the typical modification method is to add a thiol group (-SH) at its 5′ (or 3′) end [23]. However, DNA (or RNA) modified by -SH has a high price and is difficult to stand upright after embedding, making it difficult to form a three-dimensional conformation [24]. As is well known, adenosine has a considerable adsorption affinity for gold. In recent years, polyA modification methods have been widely used to bond DNA to gold surfaces due to their ability to reduce costs. Meanwhile, by controlling the number of A bases in polyA, the grafting density on the gold surface can be well controlled [25, 26].

In this work, we developed a DNA aptamer-based sandwich SPRi sensor for efficient and unlabeled detection of specific viral antigens, SARS-CoV-2 S protein, with a detection process of no more than 10 min. As shown in Fig. 1, A polyA-modified DNA aptamer was fixed on the surface of the gold film of the sensor for capturing S protein. Subsequently, AuNPs modified with the same aptamer were added to form a sandwich structure, and the LSPR generated by AuNPs under illumination was coupled with the SPR on the surface of the gold film to amplify the SPRi signal. The selected DNA aptamer has a universal high affinity for the S protein of wild-type SARS-CoV-2 and various variants Alpha, Beta, Gamma, Epsilon, Gaba, Delta, and Omicron, named MSA52 [27]. The aptamers fixed on the surface of the gold film and AuNPs are modified with $polyA_{15}$ at the 5′ end, ensuring that the embedded aptamers have a high grafting density and upright spatial configuration [25, 28]. This SPRi sensor is simple to manufacture and cost-effective and can be reused multiple times. This is the first study to detect viral marker protein using polyA-modified DNA aptamers on the SPR platform, with satisfactory sensitivity, specificity, and stability.

Experimental section

Materials and reagents

Bare gold chips were purchased from HORIBA Scientific (France). The recombinant COVID-19 B.1.1.529 (Omicron)

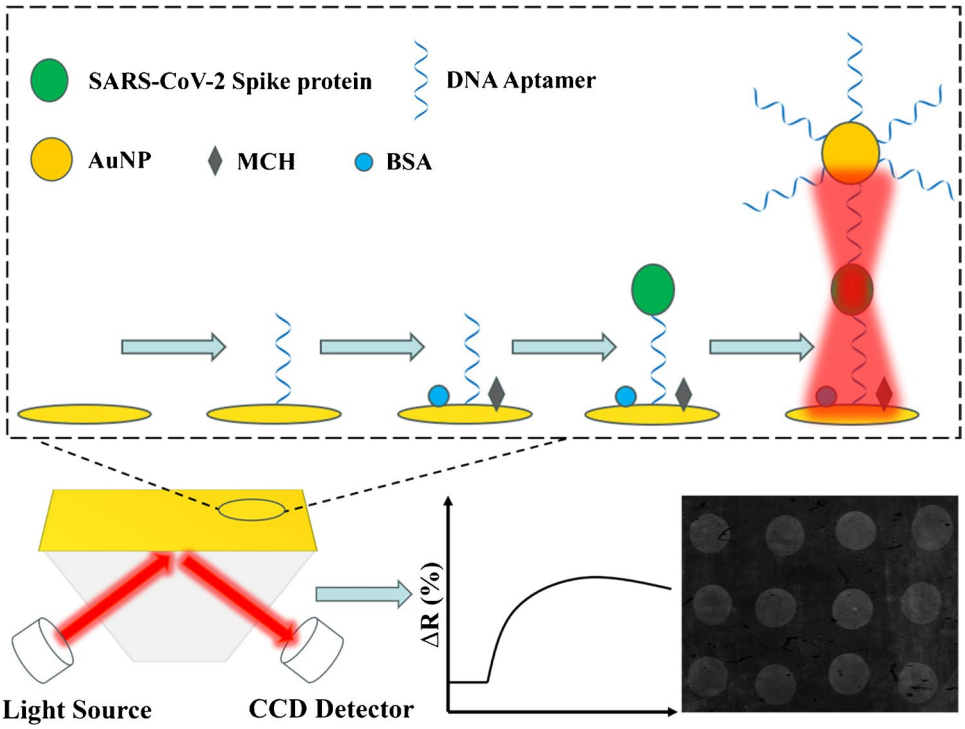

Fig. 1 Schematic diagram of the detection of SARS-CoV-2 S protein using DNA aptamer-based SPRi sensor

S1 + S2 trimer protein and MERS-CoV Spike Protein was purchased from Sino Biological, Inc. (China). Phosphate buffer solution (PBS), DNA aptamer (HPLC), and TE buffer were purchased from Sangon Biotech (China). Bovine serum albumin (BSA), human serum albumin (HAS), and lysozyme (Lys) were purchased from Solarbio (China). 6-mercapto-1-hexanol (MCH) was purchased from Aladdin. 10% SDS purchased from Phygene (Fuzhou, China). Sucrose, sodium citrate, and magnesium chloride ($MgCl_2$) were purchased from Rhawn (China). Ultrapure water was obtained from Milli-Q water (18.2 MΩ cm) system. All aptamers were heated at 95 °C for 5 min before use and then cooled at room temperature for 5 min. The information on the aptamer sequence is shown in Table S1 (Supporting information). Schreiner et al. [26] pointed out that the 15-base polyadenylate provides the best coverage and stability for DNA fixation.

Preparation of SPRi chips

Resuspend the DNA aptamer in the running buffer (0.01 M PBS + 2.5 mM $MgCl_2$), which is the sampling solution. Use a pipette to deposit the sample solution (0.3 µL/drop) onto the chip using a self-made sampling tool, which is a plastic plate with 3 × 4 array circular holes engraved on it, forming a 3 × 4 microarray. Then, incubate the SPRi biochip overnight at 25 °C and 80% relative humidity. Use ultrapure water to clean and dry briefly before use. After SPRi detection, the aptamer functionalized chip can be washed with fresh piranha solution (H_2SO_4/H_2O_2 7:3) at room temperature for 3 h to restore to a bare gold chip, and cleaned with ultrapure water before reuse.

Synthesis and modification of AuNPs

AuNPs were prepared through the classic citrate reduction method [29]. In brief, 100 mL of 0.25 mM tetrachloroauric acid solution was heated to boiling point, and then 2 mL of 1% trisodium citrate was rapidly added through intense mechanical agitation to form AuNPs. Next, the solution was continuously heated and vigorously stirred, keeping it boiling for 15 min. The color of the solution deepened and eventually turned deep red. Subsequently, stopped heating, cooled to room temperature, and stored in the dark at 4 °C.

DNA aptamers were immobilized to AuNPs using a rapid freezing method to construct DNA/AuNPs [28]. Dissolve 8 µL of DNA aptamer (100 µM) in 1 mL of AuNP solution, freeze at − 80 °C for 30 min, and thaw at room temperature. Centrifuge the obtained DNA/AuNPs twice (12,000 rpm, 5 min) to remove free DNA. Finally, the DNA/AuNPs were dispersed in the running buffer and stored in the dark at 4 °C for the next experiment. Measure the absorbance of AuNPs before and after DNA aptamer functionalization using a UV–visible spectrophotometer (TU-1901, PERSEE, Beijing). The surface morphology of AuNPs was studied by an electron transmission microscope (TEM, JEOL S0200884).

SPRi detection

The modified chips were soaked in 1 mM MCH and 5% BSA in the dark for 30 min each, washed and dried, placed on a glass prism, and then placed together in the SPRi instrument. SPRi measurement was carried out on Open PleX (HORIBA Scientific, France), which uses 810 nm light-emitting diodes (LEDs) to excite surface plasma along the entire imaging area. Select the incident angle of the light to maximize the visibility of the functionalized surface area.

All reactions were carried out in a running buffer at 25 ℃, and the flow rate was adjusted to 50 µL/min. Before each experiment, the system and SPRi chip are adjusted in the running buffer for more than 20 min, and then the array structure and the spot area to be read by the CCD are defined. The relevant area usually corresponds to the central part of the spot. Then, calibrate and standardize the CCD response of each spot by injecting 200 µL of sucrose (3 mg/mL). After injecting the running buffer to obtain the baseline, various concentrations of analytes can be injected. SPRi response reflects the binding activity occurring on the surface. Therefore, the higher the response, the higher the binding between the analyte and the aptamer. The CCD terminal outputs SPRi real-time difference image and corresponding SPRi response curve. The brightening of the spots can demonstrate effective binding between the aptamer and the target protein. After the analyte was combined, a 0.5% SDS solution for surface regeneration was used. The LOD was calculated as the average of the three background signals obtained by injecting the running buffer plus three times its standard deviation (i.e., the average value of the background signal + 3 SD).

Results and discussion

Optimization of aptamer concentration on chip surface

The detection scheme is shown in Fig. 1. The DNA aptamers were fixed on the gold film surface of the SPRi chip and then incubated with 1 mM MCH and 5% BSA in order to block non-specific adsorption. In the subsequent SPRi analysis process, the S protein injected into the instrument was captured by DNA aptamers, and the SPRi signal responses and difference images were obtained.

In this work, the concentration of DNA aptamers fixed on the gold film may affect the signal response. Therefore, we conducted experiments on different concentrations of aptamer PMA and found the ideal immobilized aptamer concentration for the following experiments. All SPRi measurements were conducted in a running buffer. As shown in Fig. 2, when 20 nM S protein was injected into the system, the aptamers of 200 nM, 400 nM, 600 nM, and 1000 nM showed quite high SPRi response values ($\Delta\% R$), but there were still significant differences among the groups: the signal of 600 nM was the highest, followed by 1000 nM, 400 nM, and 200 nM. The reason may be that when the concentration of aptamers is too high, the steric hindrance and electrostatic repulsion effects increase, thereby preventing more target proteins from being adsorbed on the chip. On the contrary, a low concentration may result in a lower grafting density, which prevents efficient binding to the target [30–32]. Therefore, in the subsequent experiments, the concentration of aptamers was used at 600 nM.

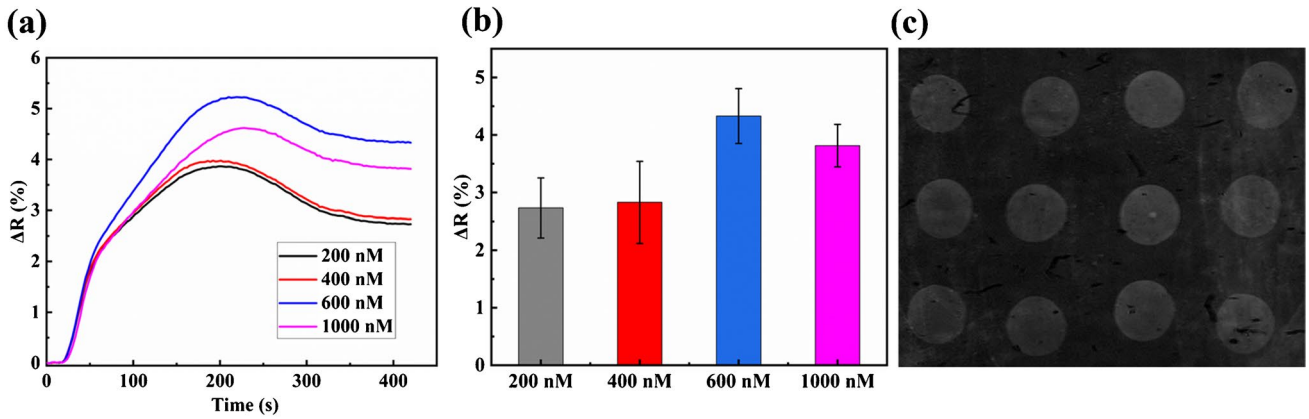

Fig. 2 When injecting S protein at a concentration of 20 nM, aptamer corresponding spots with concentrations of 200 nM, 400 nM, 600 nM, and 1000 nM of **a** SPRi sensing diagram of aptamer, **b** the signal response values, and **c** the difference image of the chip surface generated by the SPRi device for each column of aptamers from left to right

Comparison between PMA and SHMA

Because of its high affinity with a gold surface, -SH can be chemically adsorbed on the gold substrate in the form of a covalent bond, which has high stability and is usually used to fix nucleotides [33]. However, -SH-modified nucleotides may have some limitations as capture probes due to their uneven spacing and susceptibility to lodging. Research has shown that the affinity between polyA and gold can be comparable to the strong affinity of Au–S. The advantages of using base sequences containing polyA as probes include reducing non-specific adsorption and promoting the formation of upright spatial configurations [25]. This is particularly important for the adsorption of protein molecules, as they are generally large molecules and have a three-dimensional structure.

Here, the polyA-modified aptamer MSA52 (PMA) and -SH-modified MSA52 (SHMA) were immobilized on the gold film surface of the SPRi chip at a concentration of 600 nM and injected different concentrations of SARS-CoV-2 S proteins into the instrument to record the signal response. As shown in Fig. 3, the SPRi signal response values of PMA and SHMA both increase with the concentration of S protein and exhibit a linear relationship within the concentration range of 1–20 nM and 2.5–20 nM, respectively. The linear regression equations are $Y = 0.2058X + 0.0944$ and $Y = 0.1666X - 0.1367$, respectively, with correlation coefficients R^2 of 0.9926 and 0.9952. At the same concentration, the signal response values of PMA were higher than those of SHMA. The equilibrium dissociation constants (K_D) of PMA and SHMA are 0.82 (±0.03) nM and 1.27 (±0.4) nM, respectively. K_D represents the degree of dissociation between the analyte and the aptamer during equilibrium, and the smaller the K_D, the stronger the affinity between the two. Therefore, the results indicate that PolyA-modified DNA has an even slightly higher affinity to target proteins than traditional -SH modification. This may be related to the fact that PMA has a more uniform spacing after being fixed on the gold film, and can better stand upright and form a three-dimensional spatial configuration.

Direct detection analysis

After selecting the optimal experimental conditions mentioned above, the S protein of SARS-CoV-2 was directly detected without labeling using the SPRi system. The concentration of PMA fixed on the SPRi chip is selected as

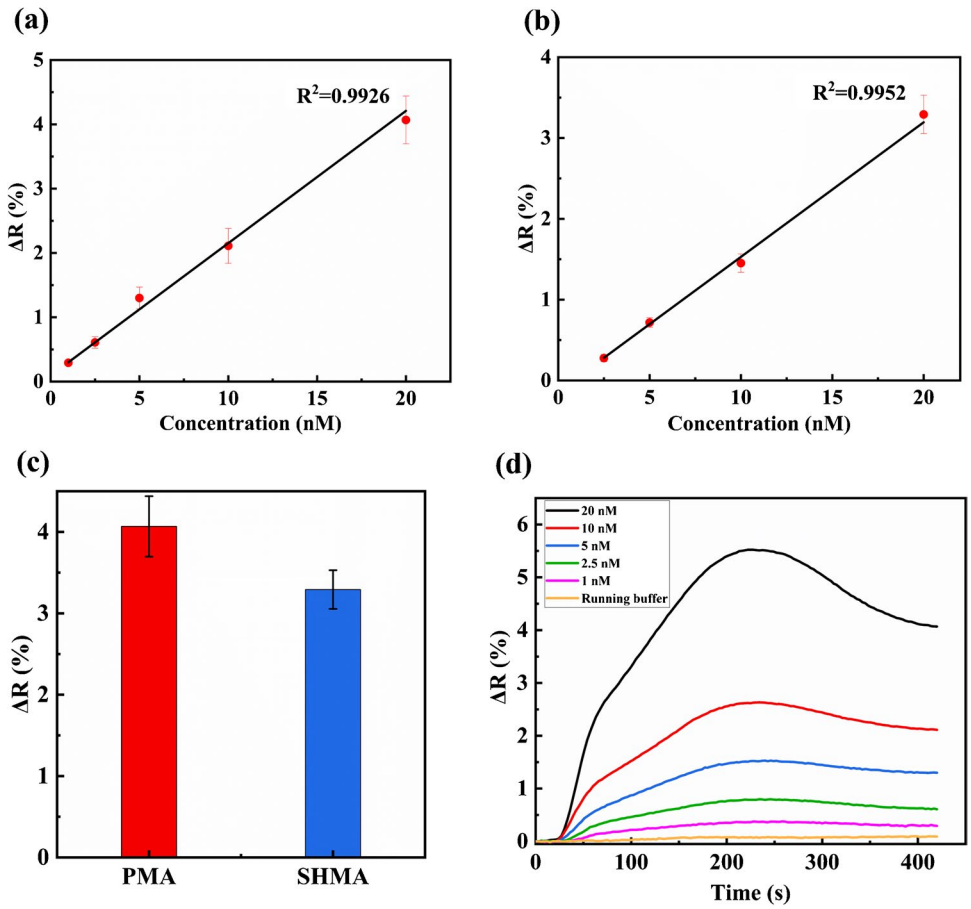

Fig. 3 **a** Linearly fitting graph of the signal response values of PMA with the concentration of S protein ($n = 3$). **b** Linearly fitting graph of the signal response values of SHMA with the concentration of S protein ($n = 3$). **c** The SPRi signal response values of PMA and SHMA at a S protein concentration of 20 nM. **d** SPRi sensing diagram for direct detection of different concentrations of S protein using PMA

600 nM, and the flow rate in the instrument is set to 50μL/min. S protein (1–20 nM) was injected into the instrument and SPRi response was recorded. As shown in Fig. 3(a) and (d), the higher the concentration of S protein, the greater the SPRi signal response value. Within the concentration range of 1–20 nM, there is a good linear relationship between signal response and concentration. The linear regression equation is $Y=0.2058X+0.0944$, and $R^2=0.9926$. The calculated K_D value is 0.82 (±0.03) nM, which indicates that the direct detection dissociation rate of the sensor is slow and the chip has good binding ability. In addition, when the signal-to-noise ratio is 3, the calculated LOD value of the sensor for detecting S protein is 0.32 nM.

Nanomaterial signal enhancement detection

In order to further improve the sensitivity of SPRi sensors and achieve lower LOD, AuNPs that can generate local surface plasmon resonance (LSPR) are used as special signal amplification probes. The principle of signal amplification is shown in Fig. 1. AuNPs modified with PMA were injected into the instrument, and the captured S proteins in the previous step were adsorbed and fixed on the chip surface, thereby enhancing the SPRi signal response.

The TEM image (Fig. 4(a)) shows that AuNPs have a uniform spherical morphology. After calculation, the particle size is approximately 17.73 ± 2.64 nm (Fig. 4(b)). This size of AuNPs can maximize their mass and electric field coupling effects, while ensuring labeling efficiency [28, 34]. As shown in Fig. 4(c), the UV–visible absorption spectrum analysis shows that the unmodified AuNPs have a maximum absorption peak at 520 nm, and the absorption peak of AuNPs red-shifted 527 nm after DNA aptamer labeling. In fact, after PMA labeling, AuNPs also underwent visible color changes to the naked eye (Fig. 4(c)). The results indicate that PMA has been successfully labeled to AuNPs, forming PMA/AuNP complexes.

Due to the inability of the sensor to directly detect significant signals for low-concentration S proteins below 1 nM, we injected PMA/AuNPs to amplify the signal after 4 min of injection of low-concentration S proteins. The experimental results show that the S protein adsorbed by PMA on the gold film can still bind to PMA/AuNPs, because one S protein has multiple RBDs [35]. As shown in Fig. 5(a), the injection of PMA/AuNPs significantly increased the SRPi signal. Among them, for the 1 nM S protein, the addition of PMA/AuNPs increased the signal by nearly 20 times (Fig. 5(b)). Meanwhile, the increased signal response value still shows a good linear relationship within the concentration range of 25–1000 pM, with a linear regression equation of $Y=0.0048X+0.1042$ and $R^2=0.9829$ (Fig. 5(c)). K_D of the interaction is calculated to be 6.39 (±0.8) pM, and when the signal-to-noise ratio is 3, the LOD is estimated to be 5.99 pM. AuNPs can generate LSPR under light, and when they are close to the gold film, they can couple with the SPR on the surface of the gold film, greatly reducing the reflected light intensity and improving the response of the SPRi sensor [36]. As mentioned earlier, polyA-modified DNA aptamers can achieve better upright effects when attached to gold surfaces, which is also true for AuNPs. Therefore, the system is very sensitive to injected PMA/AuNPs, and the designed sandwich amplification mode has achieved the expected effect.

Table S2 (Supporting information) shows the comparison between our proposed method and some of the previous detection work on SARS-CoV-2 marker protein molecules on the SPR platform. It can be observed that our detection strategy not only has the lowest level of preparation complexity, but also has obvious advantages in terms of cost and detection time. This is mainly because this scheme only uses simple modified aptamers (PMA) and relatively

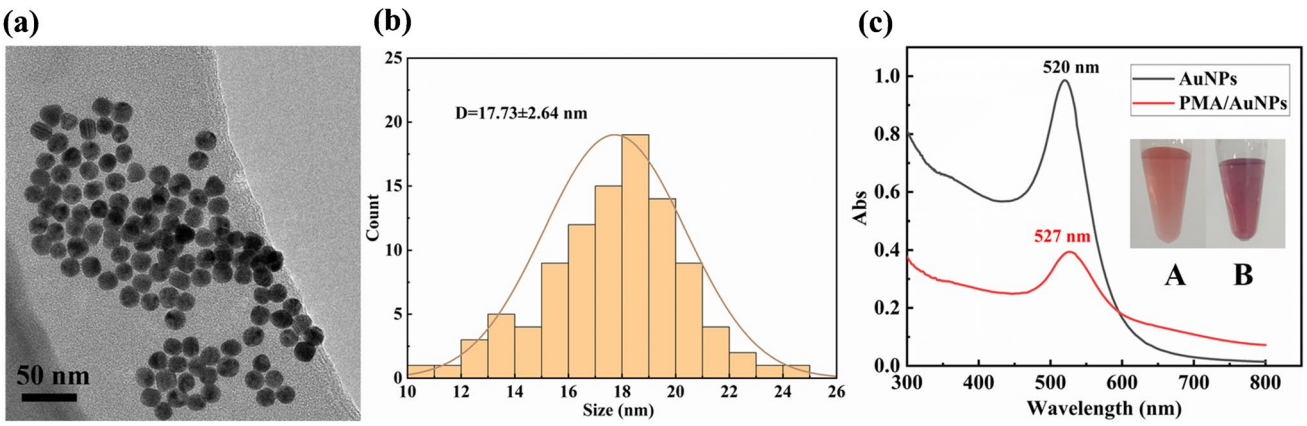

Fig. 4 **a** SEM images of AuNPs. **b** The particle size count distribution of AuNPs. **c** Ultraviolet–visible spectra of AuNPs and PMA/AuNPs (illustration A, AuNPs; B, PMA/AuNPs)

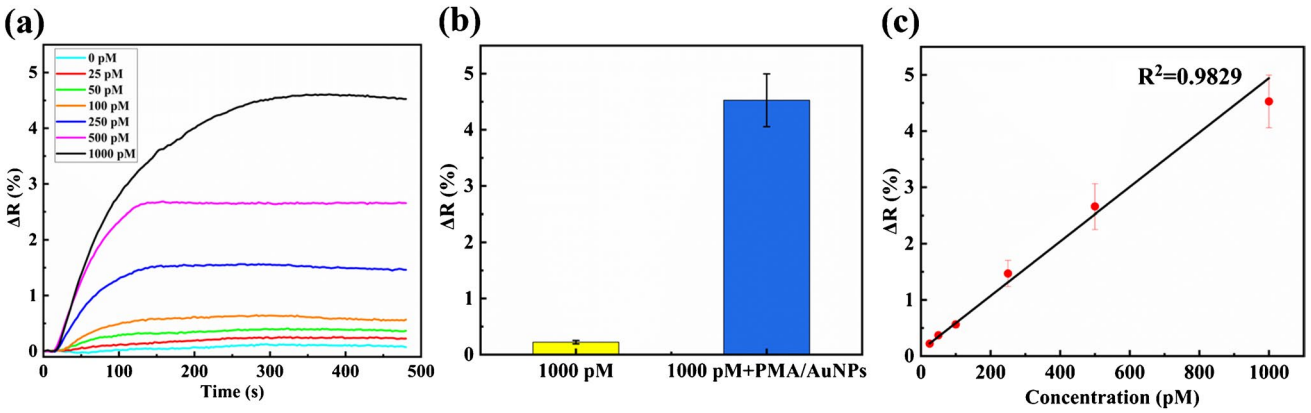

Fig. 5 **a** SPRi sensing diagram of different concentrations of S protein when adding PMA/AuNPs to amplify the signal. **b** SPRi signal response value before and after adding PMA/AuNPs to amplify the signal (S protein is 1000 pM). **c** The fitting curve between concentration and SPRi response value when adding PMA/AuNPs to amplify the signal, $R^2 = 0.9926$ ($n = 3$)

conventional nanomaterials (AuNPs) to capture target proteins and amplify SPR signals. By utilizing the advantages of polyA modification of DNA, we can functionalize both the chip surface and AuNPs with just one simple modification. This study avoids multiple modifications to the surface of the chip, nor does it require multiple composites or complex modifications to the nanomaterials, making the preparation work relatively simple. In addition, due to the simple surface modification of the chip, it can be easily recycled after detection, which also reduces costs.

Simulation calculation

In order to verify the amplification effect of AuNPs on SPRi signals in the system, the experimental system was simulated using COMSOL Multiphysics software. Based on Maxwell Garnett (MG) theory, the effective dielectric constant of each layer structure can be easily calculated [37–39]. The system is treated as a sandwiched structure composed of several layers, which is similar to the treatment in previous studies [40, 41].

The SPR reflectance curve and its slope curve before and after adding AuNPs were simulated. The result is shown in Fig. 6, the simulated data of the SPR reflectance curve and its slope curve before adding AuNPs are basically consistent with the experimental data, and the valley position is basically consistent. There are slight differences in the maximum slope, the position of the maximum slope, and their response values. These small differences might be attributed to the neglect of the presence of matching oil and the complex chemical interactions between AuNPs and the sensor. In addition, according to Fig. 6, we can also observe that the SPR reflectance curve and its slope curve have undergone significant changes before and after the addition of AuNPs, especially the response value at the maximum slope position (59.699°) has undergone significant changes before and after (an increase of 26.407%). This is clearly consistent with the phenomenon observed in the experiment and theoretically

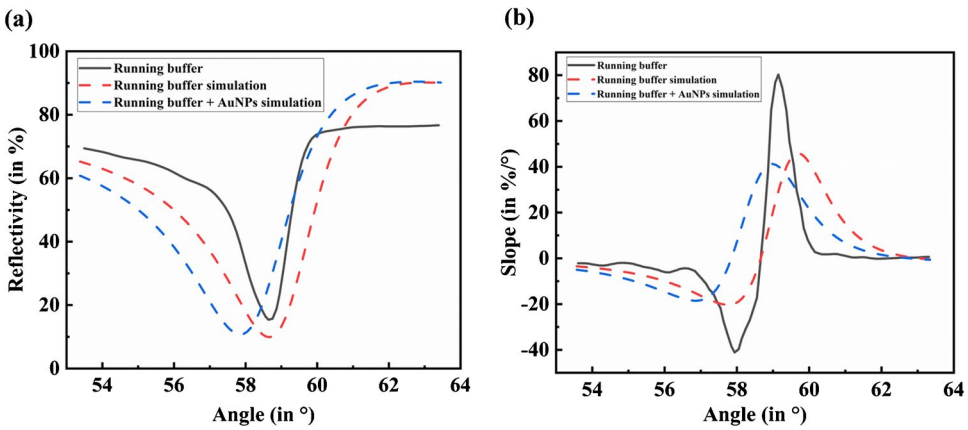

Fig. 6 **a** The SPRi reflectance curve drawn from experimental data and the SPRi reflectance curves obtained from numerical simulation before and after the addition of AuNPs. **b** The slope curves corresponding to the SPRi reflectance curves

proves that the addition of AuNPs can greatly improve the sensitivity of this sensing system.

Specificity of sensing chips

In order to verify the specificity of the designed sensor chip, we also tried to detect Middle East respiratory syndrome coronavirus S protein (MERS-S), lysozyme (Lys), bovine serum albumin (BSA), and human serum albumin (HAS), which are common protein molecules easy to interfere with the actual detection [42–44]. MERS-S was injected into the SPRi device at a concentration of 20 nM, while the concentrations of Lys, BSA, and HAS were all 40 nM, and the signal responses were recorded. As shown in Fig. 7(a) and (b), the signal response values obtained by Lys can be almost negligible. Although the signal responses of MERS-S, BSA, and HAS were slightly higher than the baseline, they were still more than an order of magnitude lower than the signal response values obtained by the SARS-CoV-2 S protein. Furthermore, even with the addition of signal enhancers PMA/AuNPs, these non-target proteins cannot achieve higher signal enhancement (Fig. 7(a) and (b)). It can be seen that SPRi sensors have high specificity, which is also due to the wide coverage area of polyA blocks [25] and the high specificity of the selected aptamer MSA52 for S protein [27].

Stability and repeatability of sensing chips

The stability, reproducibility, and reusability of biosensors are crucial for their successful application in POC. For this purpose, we conducted repeated detection experiments using 10 nM S protein. After each test, dissociate the S protein adsorbed on the chip surface with 0.5% SDS

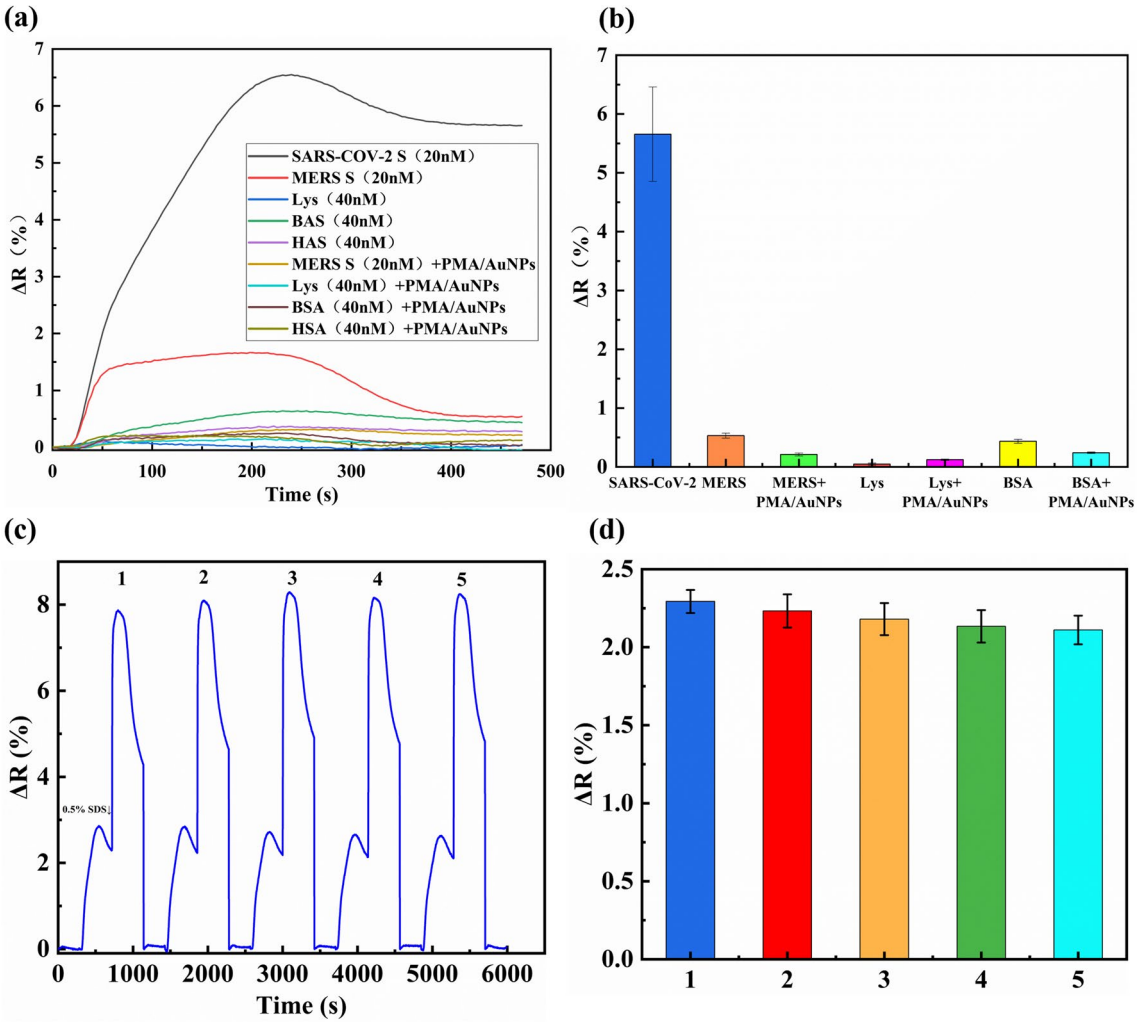

Fig. 7 **a** SPRi sensing diagram for detecting different proteins using sensors. **b** Sensors detect signal responses of different proteins ($n=3$). **c** The SPRi sensing diagram of the 10 nM S protein and its dissociation process was detected in 5 repeated experiments. **d** The signal response value of 10 nM S protein was detected 5 times in the repetitive experiment ($n=3$)

solution, then rinse with running buffer and monitor the sensor signal. After the signal has effectively recovered to the baseline, inject 10 nM of S protein again and continue monitoring the signal response, repeating this process 5 times. As shown in Fig. 7(c) and (d), it was observed that the detection signal can still reach over 90% of the initial signal after 5 cycles. This indicates that the prepared SPRi chip has good stability and reusability, which can greatly reduce the number of sensor chips used, reduce costs, and facilitate the implementation of POC.

Conclusions

SARS-CoV-2, along with other common viruses and potential new pathogens in the future, pose a threat to life, health, and economic society. Developing high sensitivity, specificity, and fast sensor systems for early detection of viral markers is crucial. In this work, we developed a simple, fast, and label-free SPRi sensor using the characteristics of DNA aptamers that are easy to modify and embed into various materials and devices, for high specificity detection of SARS-CoV-2 S protein. The recognition and capture of S protein by sensors rely on high-affinity aptamer PMA, and the addition of AuNPs significantly improves the signal response. The results of the simulation also proved this point. Before amplifying the signal, there is a good linear relationship between the signal response and concentration within the range of 1–20 nM ($R^2 = 0.9926$), and the LOD value of the SPRi sensor is 0.32 nM; after adding PMA/AuNPs, the LOD reached 5.99 pM, achieving excellent amplification effect and showing a good linear relationship in the range of 25–1000 pM ($R^2 = 0.9829$). Meanwhile, the SPRi sensor exhibits a much lower response to non-target protein molecules such as MERS-S, Lys, BSA, and HAS compared to the S protein, demonstrating its excellent specificity. In addition, after repeated use for 5 times, the sensor can still reach over 90% of the initial signal, indicating good stability and repeatability. It is worth noting that we only used a DNA aptamer (PMA) modified with PolyA to simultaneously modify chip surface and AuNPs (used to capture S proteins and amplify signals, respectively), which not only sets our detection strategy apart, but also has economic and convenient advantages. In addition, due to the simple modification of the chip surface and nanomaterials, the device is easy to manufacture and can be easily transplanted for the detection of other pathogen marker protein molecules, with only the need to find relevant suitable aptamers. This is of great significance for addressing the potential emergence of new infectious diseases. The focus of future efforts by researchers is to validate this new detection scheme with real viruses and further promote it to practical testing.

Supplementary Information The online version contains supplementary material available at https://doi.org/10.1007/s00216-024-05172-5.

Funding This work was supported by the Natural Science Foundation of Zhejiang Province under Grant No. LZ22F050004 and the National Natural Science Foundation of China under Grant Nos. 52271139, 51972292, and 22204154.

Declarations

Competing interests The authors declare no competing interests.

References

1. Morales-Narvaez E, Dincer C. The impact of biosensing in a pandemic outbreak: COVID-19. Biosens Bioelectron. 2020;163:112274. https://doi.org/10.1016/j.bios.2020.112274.
2. Orooji Y, Sohrabi H, Hemmat N, Oroojalian F, Baradaran B, Mokhtarzadeh A, et al. An overview on SARS-CoV-2 (COVID-19) and other human coronaviruses and their detection capability via amplification assay, chemical sensing, biosensing, immunosensing, and clinical assays. Nanomicro Lett. 2021;13(1):18. https://doi.org/10.1007/s40820-020-00533-y.
3. Ou X, Liu Y, Lei X, Li P, Mi D, Ren L, et al. Characterization of spike glycoprotein of SARS-CoV-2 on virus entry and its immune cross-reactivity with SARS-CoV. Nat Commun. 2020;11(1):1620. https://doi.org/10.1038/s41467-020-15562-9.
4. Walls AC, Park YJ, Tortorici MA, Wall A, McGuire AT, Veesler D. Structure, function, and antigenicity of the SARS-CoV-2 spike glycoprotein. Cell. 2020;181(2):281-92 e6. https://doi.org/10.1016/j.cell.
5. Hoffmann M, Kleine-Weber H, Schroeder S, Kruger N, Herrler T, Erichsen S, et al. SARS-CoV-2 cell entry depends on ACE2 and TMPRSS2 and is blocked by a clinically proven protease inhibitor. Cell. 2020;181(2):271-80 e8. https://doi.org/10.1016/j.cell.2020.02.052.
6. Ji T, Liu Z, Wang G, Guo X, Akbar Khan S, Lai C, et al. Detection of COVID-19: a review of the current literature and future perspectives. Biosens Bioelectron. 2020;166:112455. https://doi.org/10.1016/j.bios.2020.112455.
7. Kim H. Outbreak of novel coronavirus (COVID-19): what is the role of radiologists? Eur Radiol. 2020;30(6):3266–7. https://doi.org/10.1007/s00330-020-06748-2.
8. Suleman S, Shukla SK, Malhotra N, Bukkitgar SD, Shetti NP, Pilloton R, et al. Point of care detection of COVID-19: advancement in biosensing and diagnostic methods. Chem Eng J. 2021;414:128759. https://doi.org/10.1016/j.cej.2021.128759.
9. Conklin SE, Martin K, Manabe YC, Schmidt HA, Miller J, Keruly M, et al. Evaluation of serological SARS-CoV-2 lateral flow assays for rapid point-of-care testing. J Clin Microbiol. 2021;59(2). https://doi.org/10.1128/JCM.02020-20.
10 Kilic T, Weissleder R, Lee H. Molecular and immunological diagnostic tests of COVID-19: current status and challenges. iScience. 2020;23(8):101406. https://doi.org/10.1016/j.isci.2020.101406.
11. Wang C, Liu M, Wang Z, Li S, Deng Y, He N. Point-of-care diagnostics for infectious diseases: from methods to devices. Nano Today. 2021;37:101092. https://doi.org/10.1016/j.nantod.2021.101092.
12. Seo G, Lee G, Kim MJ, Baek SH, Choi M, Ku KB, et al. Rapid detection of COVID-19 causative virus (SARS-CoV-2) in human

nasopharyngeal swab specimens using field-effect transistor-based biosensor. ACS Nano. 2020;14(4):5135–42. https://doi.org/10.1021/acsnano.0c02823.
13. Yang Y, Peng Y, Lin C, Long L, Hu J, He J, et al. Human ACE2-functionalized gold "virus-trap" nanostructures for accurate capture of SARS-CoV-2 and single-virus SERS detection. Nanomicro Lett. 2021;13:109. https://doi.org/10.1007/s40820-021-00620-8.
14. Cennamo N, Pasquardini L, Arcadio F, Lunelli L, Vanzetti L, Carafa V, et al. SARS-CoV-2 spike protein detection through a plasmonic D-shaped plastic optical fiber aptasensor. Talanta. 2021;233:122532. https://doi.org/10.1016/j.talanta.2021.122532.
15. Yano TA, Kajisa T, Ono M, Miyasaka Y, Hasegawa Y, Saito A, et al. Ultrasensitive detection of SARS-CoV-2 nucleocapsid protein using large gold nanoparticle-enhanced surface plasmon resonance. Sci Rep. 2022;12(1):1060. https://doi.org/10.1038/s41598-022-05036-x.
16. Maria MSM. Surface plasmon resonance applications in clinical analysis. Anal Bioanal Chem. 2014;406(9–10):2303–23. https://doi.org/10.1007/s00216-014-7647-5.
17. Takemura K. Surface plasmon resonance (SPR)- and localized SPR (LSPR)-based virus sensing systems: optical vibration of nano- and micro-metallic materials for the development of next-generation virus detection technology. Biosensors (Basel). 2021;11(8). https://doi.org/10.3390/bios11080250.
18. Qu JH, Leirs K, Maes W, Imbrechts M, Callewaert N, Lagrou K, et al. Innovative FO-SPR label-free strategy for detecting anti-RBD antibodies in COVID-19 patient serum and whole blood. ACS Sens. 2022;7(2):477–87. https://doi.org/10.1021/acssensors.1c02215.
19. Huang L, Ding L, Zhou J, Chen S, Chen F, Zhao C, et al. One-step rapid quantification of SARS-CoV-2 virus particles via low-cost nanoplasmonic sensors in generic microplate reader and point-of-care device. Biosens Bioelectron. 2021;171:112685. https://doi.org/10.1016/j.bios.2020.112685.
20. Dehghani S, Nosrati R, Yousefi M, Nezami A, Soltani F, Taghdisi SM, et al. Aptamer-based biosensors and nanosensors for the detection of vascular endothelial growth factor (VEGF): a review. Biosens Bioelectron. 2018;110:23–37. https://doi.org/10.1016/j.bios.2018.03.037.
21. Ulrich H. RNA aptamers: from basic science towards therapy. Handb Exp Pharmacol. 2006;173:305–26. https://doi.org/10.1007/3-540-27262-3_15.
22. Bouchard PR, Hutabarat RM, Thompson KM. Discovery and development of therapeutic aptamers. Annu Rev Pharmacol Toxicol. 2010;50:237–57. https://doi.org/10.1146/annurev.pharmtox.010909.105547.
23. Liu B, Liu J. Freezing directed construction of bio/nano interfaces: reagentless conjugation, denser spherical nucleic acids, and better nanoflares. J Am Chem Soc. 2017;139(28):9471–4. https://doi.org/10.1021/jacs.7b04885.
24. Pei H, Li F, Wan Y, Wei M, Liu H, Su Y, et al. Designed diblock oligonucleotide for the synthesis of spatially isolated and highly hybridizable functionalization of DNA-gold nanoparticle nanoconjugates. J Am Chem Soc. 2012;134(29):11876–9. https://doi.org/10.1021/ja304118z.
25. Huertas CS, Soler M, Estevez MC, Lechuga LM. One-step immobilization of antibodies and DNA on gold sensor surfaces via a poly-adenine oligonucleotide approach. Anal Chem. 2020;92(18):12596–604. https://doi.org/10.1021/acs.analchem.0c02619.
26. Schreiner SM, Shudy DF, Hatch AL, Opdahl A, Whitman LJ, Petrovykh DY. Controlled and efficient hybridization achieved with DNA probes immobilized solely through preferential DNA-substrate interactions. Anal Chem. 2010;82(7):2803–10. https://doi.org/10.1021/ac902765g.
27. Zhang Z, Li J, Gu J, Amini R, Stacey HD, Ang JC, et al. A universal DNA aptamer that recognizes spike proteins of diverse SARS-CoV-2 variants of concern. Chemistry. 2022;28(15):e202200078. https://doi.org/10.1002/chem.202200078.
28. Hu M, Yuan C, Tian T, Wang X, Sun J, Xiong E, et al. Single-step, salt-aging-free, and thiol-free freezing construction of AuNP-based bioprobes for advancing CRISPR-based diagnostics. J Am Chem Soc. 2020;142(16):7506–13. https://doi.org/10.1021/jacs.0c00217.
29. Zhu D, Yan Y, Lei P, Shen B, Cheng W, Ju H, et al. A novel electrochemical sensing strategy for rapid and ultrasensitive detection of Salmonella by rolling circle amplification and DNA-AuNPs probe. Anal Chim Acta. 2014;846:44–50. https://doi.org/10.1016/j.aca.2014.07.024.
30. Fang Y, Jiang L, Jin S, Li Y, Jiang C, Zhang X, et al. AuNPs beacons-enhanced surface plasmon resonance imaging sensor for rapid, high-throughput and ultra-sensitive detection of three fusion genes related to acute promyelocytic leukemia. Sens Actuators B Chem. 2022;361. https://doi.org/10.1016/j.snb.2022.131728.
31. Li Y, Zou Y, Tan H, Jiang L, Fang Y, Jin S. Simultaneous and sensitive detection of two pathogenic genes of thrombotic diseases using SPRi sensor with one-step fixation probe by a poly-adenine oligonucleotide approach. Colloids Surf B Biointerfaces. 2022;209(Pt 1):112184. https://doi.org/10.1016/j.colsurfb.2021.112184.
32. Qian H, Huang Y, Duan X, Wei X, Fan Y, Gan D, et al. Fiber optic surface plasmon resonance biosensor for detection of PDGF-BB in serum based on self-assembled aptamer and antifouling peptide monolayer. Biosens Bioelectron. 2019;140:111350. https://doi.org/10.1016/j.bios.2019.111350.
33. Sperling RA, Parak WJ. Surface modification, functionalization and bioconjugation of colloidal inorganic nanoparticles. Philos Trans A Math Phys Eng Sci. 1915;2010(368):1333–83. https://doi.org/10.1098/rsta.2009.0273.
34. Hong X, Hall EA. Contribution of gold nanoparticles to the signal amplification in surface plasmon resonance. Analyst. 2012;137(20):4712–9. https://doi.org/10.1039/c2an35742a.
35. Sun M, Liu S, Song T, Chen F, Zhang J, Huang JA, et al. Spherical neutralizing aptamer inhibits SARS-CoV-2 infection and suppresses mutational escape. J Am Chem Soc. 2021;143(51):21541–8. https://doi.org/10.1021/jacs.1c08226.
36. Zeng S, Baillargeat D, Ho HP, Yong KT. Nanomaterials enhanced surface plasmon resonance for biological and chemical sensing applications. Chem Soc Rev. 2014;43(10):3426–52. https://doi.org/10.1039/c3cs60479a.
37. Ghosh SN. Electromagnetic theory and wave propagation. CRC Press. 2002.
38. Koledintseva MY, Dubroff RE, Schwartz RW. A Maxwell Garnett model for dielectric mixtures containing conducting particles at optical frequencies. Prog Electromagn Res. 2006;63:223–42. https://doi.org/10.2528/PIER06052601.
39. Ishimaru A. Electromagnetic wave propagation, radiation, and scattering: from fundamentals to applications. John Wiley & Sons. 2017.
40. Uchiho Y, Shimojo M, Furuya K, Kajikawa K. Optical response of gold-nanoparticle-amplified surface plasmon resonance spectroscopy. J Phys Chem C. 2010;114(11):4816–24. https://doi.org/10.1021/jp910438q.
41. Golden MS, Bjonnes AC, Georgiadis RM. Distance- and wavelength-dependent dielectric function of Au nanoparticles by angle-resolved surface plasmon resonance imaging. J Phys Chem C. 2010;114(19):8837–43. https://doi.org/10.1021/jp101850d.
42. Amouzadeh Tabrizi M, Nazari L, Acedo P. A photo-electrochemical aptasensor for the determination of severe acute respiratory syndrome coronavirus 2 receptor-binding domain by using

graphitic carbon nitride-cadmium sulfide quantum dots nanocomposite. Sens Actuators B Chem. 2021;345:130377. https://doi.org/10.1016/j.snb.2021.130377.
43. Wang X, Zeng Y, Zhou J, Chen J, Miyan R, Zhang H, et al. Ultrafast surface plasmon resonance imaging sensor via the high-precision four-parameter-based spectral curve readjusting method. Anal Chem. 2021;93(2):828–33. https://doi.org/10.1021/acs.analchem.0c03347.
44. Subramanian P, Lesniewski A, Kaminska I, Vlandas A, Vasilescu A, Niedziolka-Jonsson J, et al. Lysozyme detection on aptamer functionalized graphene-coated SPR interfaces. Biosens Bioelectron. 2013;50:239–43. https://doi.org/10.1016/j.bios.2013.06.026.

Publisher's Note Springer Nature remains neutral with regard to jurisdictional claims in published maps and institutional affiliations.

Springer Nature or its licensor (e.g. a society or other partner) holds exclusive rights to this article under a publishing agreement with the author(s) or other rightsholder(s); author self-archiving of the accepted manuscript version of this article is solely governed by the terms of such publishing agreement and applicable law.